Applied Physics Letters

Inorganic vacancy-ordered perovskite Cs_2SnCl_6:Bi/GaN heterojunction photodiode for narrowband, visible-blind UV detection

Cite as: Appl. Phys. Lett. **115**, 121106 (2019); https://doi.org/10.1063/1.5123226
Submitted: 03 August 2019 . Accepted: 31 August 2019 . Published Online: 17 September 2019

Dali Shao, Weiguang Zhu, Guoqing Xin, Jie Lian, and Shayla Sawyer

Applied Physics Letters ARTICLE scitation.org/journal/apl

Inorganic vacancy-ordered perovskite Cs_2SnCl_6:Bi/GaN heterojunction photodiode for narrowband, visible-blind UV detection

Cite as: Appl. Phys. Lett. **115**, 121106 (2019); doi: 10.1063/1.5123226
Submitted: 3 August 2019 · Accepted: 31 August 2019 ·
Published Online: 17 September 2019

Dali Shao,[1,a)] Weiguang Zhu,[2] Guoqing Xin,[2] Jie Lian,[2,b)] and Shayla Sawyer[1,c)]

AFFILIATIONS

[1]Electrical, Computer, and Systems Engineering Department, Rensselaer Polytechnic Institute, Troy, New York 12180, USA
[2]Department of Mechanical, Aerospace and Nuclear Engineering, Rensselaer Polytechnic Institute, Troy, New York 12180, USA

[a)]shaodali828@gmail.com
[b)]lianj@rpi.edu
[c)]sawyes@rpi.edu

ABSTRACT

A heterojunction photodiode was fabricated from Bi doped Cs_2SnCl_6 nanoparticles (Cs_2SnCl_6:Bi NPs) spin-coated on an epitaxially grown GaN substrate. With the back illumination configuration, the heterojunction photodiode demonstrated excellent narrow-band UV sensing capability with a full wavelength of half maximum of 18 nm and a maximum detectivity of 1.2×10^{12} jones, which is promising for biomedical applications. In addition to the excellent narrow band UV sensitivity, the device also demonstrated a large linear dynamic range of 71 decibels (dB) and a fast photoresponse speed (a rise time of 0.75 μs and a fall time of 0.91 μs). The excellent performance is attributed to excellent carrier separation efficiency at the heterojunction interface and improved carrier collection efficiency through the multi-walled carbon nanotube (MWCNT) network. All the above advantages are of great importance for commercial deployment of perovskite-based photodetectors.

Inorganic metal halide (IMH) perovskites have attracted significant research interest in optoelectronic applications because of their excellent material properties including the direct bandgap, strong emission, high fluorescence quantum yield, tunable bandgap covering entire UV to visible spectra, and outstanding environmental stabilities compared to organic halide perovskites (OHM).[1–7] Recently, IMH perovskites such as $Cs_2SnI_xCl_{6-x}$ and $Cs_2SnCl_{6-x}Br_x$ have been investigated for various optoelectronics applications including energy harvesting, light emitting, and light detection applications.[8–10] Remarkably, by taking advantage of the charge collection narrowing mechanism, photodetectors fabricated from $Cs_2SnCl_{6-x}Br_x$ single crystals are able to realize narrow-band sensing with a full-width at half-maximum (FWHM) of ~45 nm.[9] Narrow-band sensing photodetectors are desirable for biomedical applications such as identification of DNA, protein, and bacteria through sensing of their intrinsic fluorescence.[11,12] However, the detection bands of $Cs_2SnCl_{6-x}Br_x$ single crystal based photodetectors are restricted in the visible detection range, making them unsuitable for identification of certain protein and bacteria (such as *E. coli*) that have intrinsic fluorescence in the UV region. Cs_2SnCl_6 is a wideband gap vacancy-ordered inorganic perovskite with a bandgap of 3.9 eV, making it a promising candidate for visible-blind UV sensing applications.[13,14] Until now, the use of vacancy-ordered perovskites for optoelectronic applications such as light harvesting and photodetection is still limited due to their deteriorated carrier transport properties (e.g., too large hole mass), forbidden bandgap, and deep defect states.[15–17] Luckily, impurity doping has been demonstrated to be an effective strategy to improve the optoelectronic properties of vacancy-ordered perovskites.[10]

In this work, we demonstrate a heterojunction photodiode that is fabricated from Cs_2SnCl_6:Bi NPs spin-coated on an epitaxially grown n-GaN substrate followed by deposition of the MWCNT network on the top as the top electrode. The heterojunction photodiode exhibited outstanding narrow band sensing capability with a full-width at half-maximum (FWHM) of only 19 nm for the photoresponse spectrum. In addition, the heterojunction photodiode demonstrated promising performance including the high photocurrent to dark current ratio (~200), fast transient response (<1 μs), and excellent external quantum efficiency (68.1%). The excellent performance is attributed to efficient carrier separation at the heterojunction interface, as well as improved carrier collection efficiency originated from the multi-walled

carbon nanotube (MWCNT) network. The results in this work may trigger further research interest toward the development of perovskite based high performance visible-blind UV heterojunction photodiodes.

The Cs_2SnCl_6:Bi NPs were synthesized using the hydrothermal process. CsCl (337 mg, 2 mmol) was dissolved in 5 ml of methanol. In a separate 25 ml beaker, $SnCl_4{\cdot}5H_2O$ (351 mg, 1 mmol) with $BiCl_3$ (31.5 mg, 0.1 mmol) was mixed and dissolved in 5 ml of methanol to afford a clear transparent solution. The addition of the alcoholic mixture solution to the CsCl solution under vigorous stirring at room temperature led to spontaneous precipitation of white powder. The mixture was stirred for a further 30 min to ensure completion of the reaction, after which the solid was washed with methanol in a centrifuge at 3000 RPM for 5 min twice. Then, the obtained powder (Cs_2SnCl_6:Bi NPs) was dried in an oven at 80 °C overnight.

The X-ray diffraction (XRD) patterns of the Bi doped (red line) and undoped (blue line) were measured using a Bruker D8-Discover X-ray diffractometer, as shown in Fig. 1(a). The major XRD peak position of Cs_2SnCl_6:Bi NPs has been slightly shifted to lower 2θ values as compared to the undoped Cs_2SnCl_6 NPs. This shift is due to the substitution of Sn of ionic radius 83 pm by atoms Bi that have a larger ionic radius of 117 pm. The Bi doping concentration is determined to be ~4.8%. Figure 1(b) illustrates the crystal structure of Cs_2SnCl_6, which represents a vacancy-ordered double perovskite structure with isolated [SnCl6] octahedra. The UV-visible absorption spectrum of the Cs_2SnCl_6:Bi NPs and the UV-visible transmission spectrum of the GaN substrate were measured using a Shimadzu UV-Vis 2550 spectrophotometer and are presented in Fig. 1(c). The Cs_2SnCl_6:Bi NPs show a sharp optical absorption edge at ~315 nm (3.9 eV) and an additional sub-bandgap absorption band centered at 375 nm (3.3 eV). The 315 nm peak originates from intra band transition from the valence band maximum (VBM) to the conduction band minimum (CBM). The additional 375 nm absorption peak would be assigned to transition from the new VBM (VBM') consisting of Cl 3p and Bi 6s orbitals to the Cs_2SnCl_6 host CBM due to the Bi doping,[10] as illustrated in the schematic energy diagram in Fig. 1(d). Note that this additional subbandgap absorption band of Cs_2SnCl_6:Bi NPs is essential for the narrow-band UV sensing capability of this heterojunction photodiode as it has an ~40 nm wavelength overlap with the transmission spectrum of the GaN substrate (with a cutoff wavelength of 360 nm), as shown in the shaded area of Fig. 1(c).

The three-dimensional schematic illustration of the Cs_2SnCl_6:Bi/GaN heterojunction photodiode is shown in Fig. 2(a). The GaN substrate consists a 0.5 μm epitaxial GaN layer doped with Si (5×10^{17} cm^{-3}) grown on top of a 3 μm semi-insulating GaN buffer layer and a 330 μm double side polished c-plane sapphire substrate. The synthesized Cs_2SnCl_6:Bi NPs were dispersed in dichlorobenzene solvent and spin coated to the GaN substrate at 1500 RPM three times. The thickness of the spin-coated Cs_2SnCl_6: Bi NP thin film is ~1.2 μm. MWCNTs with a carboxyl functionalized group were then dispersed in dimethylformamide (DMF) and drop cast onto the top of the Cs_2SnCl_6:Bi NP thin film as the top electrode. As has been discussed in our previous work, the MWCNT network typically has a low sheet resistance (~50 Ω/square) and can uniformly cover the surface of the active layer and hence dramatically improve the carrier collection efficiency.[18] An Au contact with a thickness of 150 nm was deposited on the GaN substrate using E-beam evaporation through a shadow mask. The active device area is 0.01 cm^2 defined by the shadow mask. Finally, the photodetector was packaged and wire bonded using Epo-Tek H20E conductive epoxy. The schematic energy band diagram of the heterojunction photodiode under the reverse bias condition is shown in Fig. 2(b), which shows that the band structure at the perovskite-GaN heterointerface benefits the separation of photogenerated electron-hole pairs, resulting in the high photocurrent and

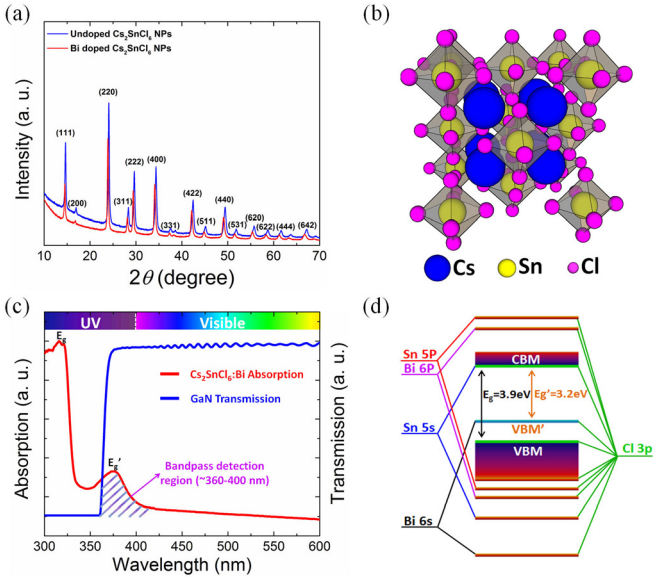

FIG. 1. (a) XRD patterns of Bi doped and undoped Cs_2SnCl_6:Bi NPs. (b) The crystal structure of the vacancy-ordered double perovskite Cs_2SnCl_6. (c) UV-visible absorption spectrum of the Cs_2SnCl_6:Bi NPs (red) and the transmission spectrum of the GaN substrate. (d) Schematic energy diagram for Bidoped Cs_2SnCl_6 NPs.[10]

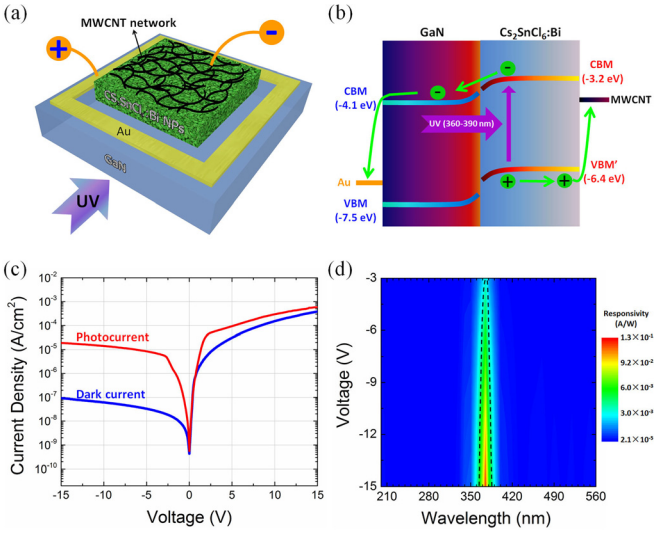

FIG. 2. (a) Three-dimensional schematic illustration of the Cs_2SnCl_6:Bi/GaN heterojunction photodiode. (b) Schematic energy band diagram showing the carrier dynamics in the interfacial region of the heterojunction. (c) Photocurrent and dark current density of the heterojunction photodiode. (d) Pseudocolor maps of photoresponsivity spectra of this heterojunction photodiode measured with varying bias voltages.

responsivity. To investigate the photoresponse of the device, the I-V characteristics of the photodetector were measured using a HP4155B semiconductor parameter analyser and a UV LED with a center peak wavelength of 375 nm, as shown in Fig. 2(c). The heterojunction photodiode shows excellent rectifying characteristics with a high rectification ratio of 345 when biased at ±2V. When forward biased (defined as adding positive voltage on the GaN substrate), the dark current increases exponentially following the equation $I \sim \exp(\alpha V)$, which is usually observed in the wideband gap p-n heterojunctions due to a recombination-tunneling mechanism.[19–21] The constant α was evaluated to be 0.21 V^{-1} by fitting the experimental data. Upon turning on the 375 nm UV light (backside illumination from the GaN side), the photocurrent is more than two orders of magnitude higher than dark current under reverse bias conditions, demonstrating a high signal to noise ratio. The photoresponsivity pseudocolor map of the device as a function of bias voltages was measured using a Shimadzu UV-Vis 2550 spectrophotometer in connection with an optical power meter, as presented in Fig. 2(d). A maximum photoresponsivity of 208 mA/W is achieved within a very narrow band centered at a wavelength of 378 nm, corresponding to an external quantum efficiency (EQE) of 68.1%. The high EQE is attributed to the high carrier separation efficiency at the Cs_2SnCl_6:Bi/GaN heterointerface as well as excellent carrier collection efficiency from the MWCNT network. It is worth mentioning that the EQE of this device can be further improved by optimizing the thickness of the Cs_2SnCl_6: Bi NP film, which can effectively reduce the charge recombination loss of the photogenerated carriers during their transport to the electrodes while at the same time ensure a reasonable amount of light energy absorbed in the active layer for the photogeneration process. The device performance optimization regarding the thickness of the Cs_2SnCl_6 thin film will be conducted in our future work for biodetection system integrations.

The full width at half maximum (FWHM) of this narrow band photoresponse is determined to be 18 nm, demonstrating a highly selective photoresponse of this photodetector. It is worth mentioning that the center peak wavelength and FWHM of the photoresponse spectrum of this device can by tuned by using $Al_xGa_{1-x}N$ as the substrate, whose bandgap can be tailored from 3.4 eV to 6.4 eV with varying Al compositions. Such great tunability of the photoresponse spectrum is highly desirable for biomedical applications such as identification of DNA, protein, and bacteria through sensing of their intrinsic fluorescence.

The transient photoresponse of the heterojunction UV photodetector was measured under a 375 nm short pulse (100 kHz) light from a LED, as presented in Fig. 3(a) The rise time (output signal changing from 10% to 90% of the peak output value) and the decay time (output signal changing from 90% to 10% of the peak output value) of the photocurrent are 0.75 μs and 0.91 μs, respectively. This is faster than most of the perovskite based photodetectors reported so far, indicating a good quality of the synthesized Cs_2SnCl_6:Bi NPs as the photogenerated carriers at the heterointerface can transport through the NP thin film quickly.[22–27] For practical applications, such as image sensors and illumination meters, we need to extract the intensity of the detection light from the photocurrent over a wide light-intensity range, and so having a constant responsivity over a wide range of light intensities is an important figure of merit for a photodetector. The linear dynamic range (LDR) of a photodetector indicates that within a certain range, the photodetector has a linear response to varying incident light intensities and can maintain a constant responsivity. LDR is expressed as[28,29]

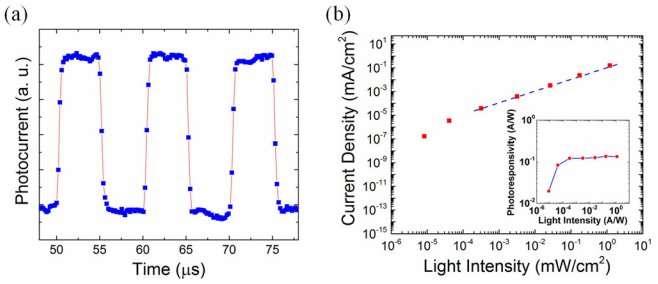

FIG. 3. (a) Transient response of the Cs_2SnCl_6:Bi/GaN heterojunction photodiode with a rising time of 0.75 μs and a falling time of 0.91 μs measured under ambient conditions.

$$\mathrm{LDR} = 20\log(P_{sat}/P_{low}),$$

where P_{sat} and P_{low} are the upper and lower limits of the incident light intensities; beyond this range, the photocurrent begins to deviate from linearity. The LDR of the heterojunction photodiode was characterized by measuring the photocurrent at a fixed frequency of 10 Hz under 375 nm UV illumination upon varying light intensity from 1.2×10^{-3} W/cm^2 to 8.3×10^{-9} W/cm^2, as shown in Fig. 3(a). Our device demonstrated a linear photoresponse within the light intensity range of 1.2×10^{-3} W/cm^2 to 3.2×10^{-7} W/cm^2, corresponding to a LDR of ~71 dB. This is better than GaN photodetectors (50 dB) and InGaAs photodetectors (66 dB).[29] The inset of Fig. 3(b) shows the photoresponsivity measured within the above light intensity range, which shows a good consistency of the responsivity with the light intensity range of 1.2×10^{-3} W/cm^2 to 3.2×10^{-7} W/cm^2.

The specific detectivity is one of the most important figure-of-merits for photodetectors. It characterizes the capability of a photodetector to detect the weakest light signal. The specific detectivity (D^*) can be expressed as[29]

$$\mathrm{D}^* = \frac{(AB)^{1/2}}{\mathrm{NEP}},$$

where the NEP $= i_n/R$ is the noise equivalent power, B is the bandwidth, A is the area of the device, i_n is the measured noise current, and R is the photoresponsivity of the photodetector. The total noise current of the photodetector was directly measured using an SR830 lock-in amplifier at different dark current levels and at various frequencies (range of 1 Hz–5 kHz), as presented in Fig. 4. The noise current is dominated by shot noise and is not sensitive to frequency modulation, indicating a negligible 1/f noise of the device. A maximum specific detectivity of 1.2×10^{12} jones is achieved for this heterojunction photodiode at 378 nm, demonstrating an excellent sensitivity for ultraviolet detection.

In summary, we developed a heterojunction photodiode by deposition of a wideband gap, vacancy-ordered double perovskite NP thin film on the GaN substrate. The heterojunction photodiode demonstrated excellent narrow-band UV sensing capability with a full wavelength of half maximum of 19 nm. In addition, the device shows high responsivity/EQE and fast transient photoresponse, which are attributed to excellent carrier separation efficiency at the heterojunction interface and improved carrier collection efficiency through the MWCNT network. The results in this work can be of particular

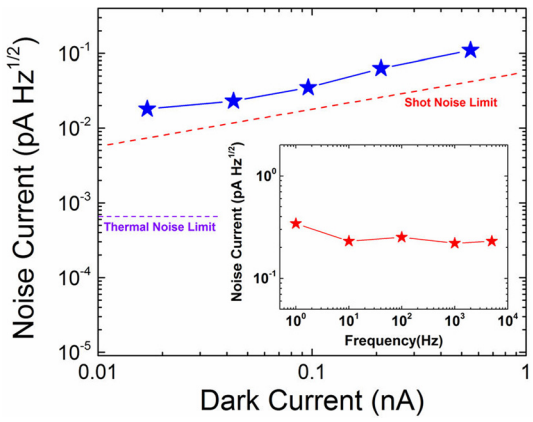

FIG. 4. Photocurrent measured with varying light intensities. Inset: photoresponsivity measured with varying light intensities.

interest for the development of high performance UV photodetectors for biomedical applications.

Dr. Sawyer and Dr. Shao acknowledge funding support from the New Knowledge and Innovation Program (KIP) Seed Grant program at Rensselaer Polytechnic Institute. Dr. Lian acknowledges the support from the Center for Performance and Design of Nuclear Waste Forms and Containers, an Energy Frontier Research Center funded by the U.S. Department of Energy, Office of Science, Basic Energy Sciences under Award # No. DE-SC0016584.

REFERENCES

[1]M. Kulbak, D. Cahen, and G. Hodes, J. Phys. Chem. Lett. **6**, 2452 (2015).
[2]A. Swarnkar, A. R. Marshall, E. M. Sanehira, B. D. Chernomordik, D. T. Moore, J. A. Christians, T. Chakrabarti, and J. M. Luther, Science **354**, 92 (2016).
[3]L. Protesescu, S. Yakunin, M. I. Bodnarchuk, F. Krieg, R. Caputo, C. H. Hendon, R. X. Yang, A. Walsh, and M. V. Kovalenko, Nano Lett. **15**, 3692 (2015).
[4]J. Song, J. Li, X. Li, L. Xu, Y. Dong, and H. Zeng, Adv. Mater. **27**, 7162 (2015).
[5]X. Zhang, B. Xu, J. Zhang, Y. Gao, Y. Zheng, K. Wang, and X. W. Sun, Adv. Funct. Mater. **26**, 4595 (2016).
[6]X. Li, Y. Wu, S. Zhang, B. Cai, Y. Gu, J. Song, and H. Zeng, Adv. Funct. Mater. **26**, 2435 (2016).
[7]N. Yantara, S. Bhaumik, F. Yan, D. Sabba, H. A. Dewi, N. Mathews, P. P. Boix, H. V. Demir, and S. Mhaisalkar, J. Phys. Chem. Lett. **6**, 4360 (2015).
[8]B. Lee, C. C. Stoumpos, N. Zhou, F. Hao, C. Malliakas, C.-Y. Yeh, T. J. Marks, M. G. Kanatzidis, and R. P. H. Chang, J. Am. Chem. Soc. **136**, 15379 (2014).
[9]J. Zhou, J. Luo, X. Rong, P. Wei, M. S. Molokeev, Y. Huang, J. Zhao, Q. Liu, X. Zhang, J. Tang, and Z. Xia, Adv. Opt. Mater. **7**, 1900139 (2019).
[10]Z. Tan, J. Li, C. Zhang, Z. Li, Q. Hu, Z. Xiao, T. Kamiya, H. Hosono, G. Niu, E. Lifshitz, Y. Cheng, and J. Tang, Adv. Funct. Mater. **28**, 1801131 (2018).
[11]L. Li, Y. Deng, C. Bao, Y. Fang, H. Wei, S. Tang, F. Zhang, and J. Huang, Adv. Opt. Mater. **5**, 1700672 (2017).
[12]S. Rajamani, K. Arora, A. Konakov, A. Belov, D. Korolev, A. Nikolskaya, A. Mikhaylov, S. Surodin, R. Kryukov, D. Nikolitchev, A. Sushkov, D. Pavlov, D. Tetelbaum, M. Kumar, and M. Kumar, Nanotechology **29**, 305603 (2018).
[13]A. E. Maughan, A. M. Ganose, D. O. Scanlon, and J. R. Neilson, Chem. Mater. **31**, 1184 (2019).
[14]Y. Cai, W. Xie, H. Ding, Y. Chen, K. Thirumal, L. H. Wong, N. Mathews, S. G. Mhaisalkar, M. Sherburne, and M. Asta, Chem. Mater. **29**, 7740 (2017).
[15]Z. Xiao, W. Meng, J. Wang, D. B. Mitzi, and Y. Yan, Mater. Horiz. **4**, 206 (2017).
[16]Z. Xiao and Y. Yan, Adv. Energy Mater. **7**, 1701136 (2017).
[17]Z. Xiao, Z. Song, and Y. Yan, Adv. Mater. **31**, 1803792 (2019).
[18]D. Shao, M. Yu, J. Lian, and S. Sawyer, Appl. Phys. Lett. **102**, 021107 (2013).
[19]J. B. Fedison, T. P. Chow, H. Lu, and I. B. Bhat, Appl. Phys. Lett. **72**, 2841 (1998).
[20]R. Ghosh and D. Basak, Appl. Phys. Lett. **90**, 243106 (2007).
[21]D. Shao, M. Yu, J. Lian, and S. Sawyer, Appl. Phys. Lett. **101**, 211103 (2012).
[22]X. Wu, B. Zhou, J. Zhou, Y. Chen, Y. Chu, and J. Huang, Small **14**, 1800527 (2018).
[23]H. Sun, W. Tian, F. Cao, J. Xiong, and L. Li, Adv. Mater. **30**, 1706986 (2018).
[24]H. Zhou, Z. Song, P. Tao, H. Lei, P. Gui, J. Mei, H. Wang, and G. Fang, RSC Adv. **6**, 6205 (2016).
[25]M. Zhang, F. Zhang, Y. Wang, L. Zhu, Y. Hu, Z. Lou, Y. Hou, and F. Teng, Sci. Rep. **8**, 11157 (2018).
[26]W. B. Fu, G. L. Shang, X. X. Gong, L. D. Zhang, and G. T. Fei, J. Mater. Chem. C **5**, 1471 (2017).
[27]P. Tan, B. Chen, H. Xu, W. Cai, W. He, M. Liu, Z. Shao, and M. Ni, Small **14**, 1800225 (2018).
[28]L. Dou, Y. Yang, J. You, Z. Hong, W.-H. Chang, G. Li, and Y. Yang, Nat. Commun. **5**, 5404 (2014).
[29]C. Bao, Z. Chen, Y. Fang, H. Wei, Y. Deng, X. Xiao, L. Li, and J. Huang, Adv. Mater. **29**, 1703209 (2017).